Tectonophysics xxx (2013) xxx–xxx

Contents lists available at SciVerse ScienceDirect

Tectonophysics

journal homepage: www.elsevier.com/locate/tecto

Quantifying the thermo-mechanical impact of plume arrival on continental break-up

Sascha Brune [a,*], Anton A. Popov [b], Stephan V. Sobolev [a,c]

[a] German Research Centre for Geosciences, Potsdam, Telegrafenberg, 14473 Potsdam, Germany
[b] Institute of Geosciences, Johannes Gutenberg University Mainz, D-55099 Mainz, Germany
[c] Schmidt Institute of Physics of the Earth, B. Gruzinskaya 10, Moscow, Russia

ARTICLE INFO

Article history:
Received 5 March 2012
Received in revised form 26 December 2012
Accepted 1 February 2013
Available online xxxx

Keywords:
Rifting
Continental break-up
Plume–lithosphere interaction
Lithosphere erosion
Numerical modeling
Tectonic forces

ABSTRACT

The arrival of a plume head at Earth's continental lithosphere is often considered to be an important factor for continental break-up. However, the impact of plume impingement on strength and duration of a rift remains unclear. In this study, we quantify the mechanical and thermal influence of a plume (i.e. lithosphere erosion) on continental break-up. To do that we apply the three-dimensional numerical code SLIM3D that features realistic elasto-visco-plastic rheology. We model the thermo-mechanical response of a segment of Earth's lithosphere that is affected both by extension as well as plume-related lithosphere erosion in order to evaluate the influence on the overall force budget. We find that lithosphere erosion leads to a moderate lithospheric strength reduction of several TN/m. In a force-limited environment, however, this strength reduction may have strong influence on the timing of continental break-up, or it may even control whether continental break-up takes place at all. Additional reduction of the lithospheric strength is likely due to the massive emplacement of dikes that follows intensive melting within the plume head.

1. Introduction

Continental rifting is driven by plate boundary forces, mantle drag and gravitational potential. If extension persists long enough to achieve full splitting of the continental lithosphere a new ocean is formed and the rift is termed successful. The duration of extension before complete break-up may vary by two orders of magnitude from several My up to some 100 My (Ziegler and Cloetingh, 2004), whereby in some cases the break-up is triggered by plume arrival. Although mantle plumes are not a necessary prerequisite for rifting, they do have decisive impact on the success of a rift system (Courtillot et al., 1999). Ziegler and Cloetingh (2004) compiled rift durations of both aborted and successful rifts. We appended two rifts to their rift compilation (Fig. 1) and added relevant Large Igneous Provinces over Phanerozoic history (Courtillot and Renne, 2003) and other plume-related volcanic events. Of those rifts that did not experience plume arrival, about one third resulted in break-up while the others became inactive. All 8 rifts however where plume involvement is evident or hypothesized have become successful. Note that in many cases, there is a distinct delay between plume arrival and continental break-up.

The arrival of a plume head at the lithosphere often involves large amounts of melts which penetrate into the lithosphere. If mafic melt crystallizes within the lithosphere it heats the surroundings and at the same time forms dense eclogite bodies. Both mechanisms promote Rayleigh–Taylor instability and induce foundering of the lower lithosphere (Elkins-Tanton and Hager, 2000; Sobolev et al., 2011). This process of lithosphere erosion results in successive ascension of the plume head and repeats until mafic melts crystallize to light garnet-free rocks of neutral or even positive buoyancy that inhibit the recurrence of Rayleigh–Taylor instability.

During the last decade, numerical methods have become sufficiently efficient to elucidate detailed questions on interaction between plume head and lithosphere: The evolution of plume impingement has been studied using different rheological stratifications of the lithosphere (Burov and Guillou-Frottier, 2005; Burov et al., 2007; d'Acremont et al., 2003). These models show that complex spatio-temporal topographic patterns can be created during interaction of plume-head and relatively thin lithosphere. Another study (Ueda et al., 2008) addresses Archean subduction initiation due to a thermo-chemical plume head. Both the buoyancy of the plume head and the volatile-induced reduction of plastic lithospheric strength appear to be essential for the initiation of self-consistent subduction. Plume composition has strong influence on lithospheric weakening and subsequent erosion. Especially eclogitization of mafic intrusions promotes foundering of the lower lithosphere. Numerical modeling of the Siberian plume arrival showed that large amounts (15 wt.%) of recycled oceanic crust in the plume explain well the absence of km-scale pre-magmatic uplift in Siberia as well as massive volcanic degassing leading to the Permian mass extinction (Sobolev et al., 2011). Despite the obviously 3D nature of a plume head, no 3D numerical model of plume-head lithosphere interaction has been published so far.

Although many numerical models addressed continental rifting and break-up (e.g. Bassi, 1991; Behn et al., 2002; Braun and Beaumont, 1989; Buck, 1991; Buiter et al., 2008; Burov and Cloetingh, 1997; Huismans and Beaumont, 2003, 2011; Lavier and Manatschal, 2006;

* Corresponding author. Tel.: +49 3312881928.
E-mail address: brune@gfz-potsdam.de (S. Brune).

0040-1951/$ – see front matter © 2013 Elsevier B.V. All rights reserved.
http://dx.doi.org/10.1016/j.tecto.2013.02.009

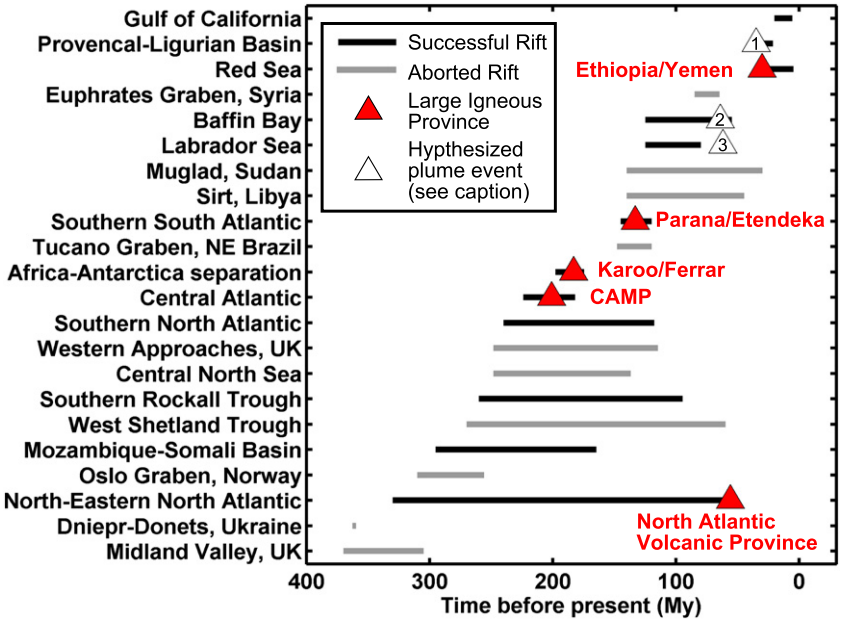

Fig. 1. Compilation of rift duration and plume arrival, largely based on Ziegler and Cloetingh (2004) and Courtillot and Renne (2003), respectively. Additional data for the South Atlantic come from Moulin et al. (2010) and for Africa–Antarctica separation from Golonka and Bocharova (2000). Hypothesized plume events comprise (1) a plume below the Western Mediterranean (Bell et al., 2004) inferred from chemical data of Italian rocks; (2) the West Greenland Volcanic Province (Gill et al. 1995); and (3) Paleocene volcanism in the Labrador Sea due to the proto-Icelandic plume (Chalmers et al., 1995).

Lavier et al., 2000; Regenauer-Lieb et al., 2006; Rey et al., 2011; Schmeling, 2010; van Wijk and Cloetingh, 2002; Zuber and Parmentier, 1986), due to limited capabilities of computational resources, three-dimensional models became feasible only recently. These models can be grouped in three categories: (1) Crustal-scale models that allow for relatively high resolution are used to compute structural aspects of a rift system (Allken et al., 2011, 2012; Katzman et al., 1995). However, these kinds of models are limited to the initial rift stage, where the influence of a deforming mantle lithosphere is negligible. (2) Models involving both crust and mantle lithosphere and having somewhat lower resolution, can be applied to initial and intermediate rift stages (Dunbar and Sawyer, 1996; Le Pourhiet et al., 2012; van Wijk, 2005; van Wijk and Blackman, 2005). These experiments, however feature certain limitations of their own, since they do not involve asthenospheric rheology which becomes important during later rift stages and break-up. (3) Most recently three-dimensional thermo-mechanical rift models involved crust, lithospheric mantle as well as asthenospheric mantle. Gac and Geoffroy (2009) studied the impact of melt-related soft points within an extending lithosphere. The resulting crustal structures agree well with observed zig-zag patterns at volcanic passive margins. Brune et al. (2012) investigated the forces that are required to maintain a certain rift velocity. A simple analytical model showed that oblique rifting requires less force than rift-perpendicular extension. This conclusion was corroborated by further lithospheric-scale numerical modeling. Using an extended version of this model together with a novel stress-visualization technique, the structural evolution of oblique rifts has been addressed from initial rifting to continental break-up (Brune, submitted for publication). Moreover, 3D numerical models successfully reproduced fundamental features of oceanic spreading systems (Choi et al., 2008; Gerya, 2010, 2013).

It is plausible that plume–lithosphere interaction in an ongoing rift system promotes continental break-up. Little is known, however about the size of the lithosphere erosion region and its significance for continental break-up. Therefore, we investigate how the geometry of the erosion-affected lithospheric area influences the break-up process and we evaluate the impact of lithosphere erosion on the rift evolution in a force-limited setting. In particular we address a number of possible plume-related weakening processes like (1) lithosphere erosion from below, (2) strong local temperature increase in the crust, as well as (3) thermally induced isostatic uplift and study how the lithospheric strength is affected by these processes in the course of rift evolution.

2. Numerical techniques

We use the three-dimensional, implicit, finite element code SLIM3D (Semi-Lagrangian Implicit Model for 3 Dimensions, (Popov and Sobolev, 2008)) to solve the thermo-mechanically coupled conservation equations of

Momentum

$$-\frac{\partial p}{\partial x_i}+\frac{\partial \tau_{ij}}{\partial x_j}+\rho g_i=0 \tag{1}$$

Energy

$$\rho C_p\frac{DT}{Dt}=\frac{\partial}{\partial x_i}\left(\lambda\frac{\partial T}{\partial x_i}\right)+\tau_{ij}\dot{\varepsilon}_{ij}+\rho A \tag{2}$$

and Mass

$$\frac{1}{K}\frac{Dp}{Dt}-\alpha_T\frac{DT}{Dt}+\frac{\partial v_i}{\partial x_i}=0 \tag{3}$$

with pressure p, coordinates x_i, time t, stress deviator τ_{ij}, density ρ, gravity vector g_i, heat capacity C_p, temperature T, material time derivative D/Dt, heat conductivity λ, strain rate deviator $\dot{\varepsilon}_{ij}$, radioactive heat production A, bulk modulus K, thermal expansivity α_T, and velocities v_i. The Einstein summation rule applies for repeated indices. Parameter values are shown in Table 1.

We use the Galerkin procedure of the Finite Element Method to solve the system of equations for the primary variables, namely incremental displacement (Δu), and temperature (T). Multiple remeshing

Please cite this article as: Brune, S., et al., Quantifying the thermo-mechanical impact of plume arrival on continental break-up, Tectonophysics (2013), http://dx.doi.org/10.1016/j.tecto.2013.02.009

Table 1
Model parameters. Dislocation creep parameters for upper crust: wet quartzite (Gleason and Tullis, 1995), lower crust: Pikwitonian granulite (Wilks and Carter, 1990), lithospheric mantle: dry olivine (Hirth and Kohlstedt, 2003), astheonspheric mantle: wet olivine, i.e. 500 ppm H/Si (Hirth and Kohlstedt, 2003). Peierls creep parameters for mantle: (Kameyama et al., 1999). *the friction coefficient decreases linearly by 90% of the initial value when plastic strain reaches 1, and remains constant for larger strains.

Parameter	Upper crust	Lower crust	Strong mantle	Weak mantle
Density, ρ (kg m^{-3})	2700	2850	3300	3300
Thermal expansivity, α_T (10^{-5} K^{-1})	2.7	2.7	3.0	3.0
Bulk modulus, K (GPa)	55	63	122	122
Shear modulus, G (GPa)	36	40	74	74
Heat capacity, C_p (J kg^{-1} K^{-1})	1200	1200	1200	1200
Heat conductivity, λ (W K^{-1} m^{-1})	2.5	2.5	3.3	3.3
Radiogenic heat production, A (μW m^{-3})	1.5	0.2	0	0
Initial friction coefficient, μ (−)	0.6	0.6	0.6	0.6
Maximum plastic friction softening*	90%	90%	None	None
Cohesion, c (MPa)	5.0	5.0	5.0	5.0
Pre-exponential constant for diffusion creep, $\log(B_{Diff})$ (Pa^{-1} s^{-1})	–	–	−8.65	−8.65
Activation energy for diffusion creep, E_{Diff} (kJ/mol)	–	–	375	335
Activation volume for diffusion creep, V_{diff} (cm^{-3}/mol)	–	–	6	4
Pre-exponential constant for dislocation creep, $\log(B_{Disloc})$ (Pa^{-n} s^{-1})	−28.0	−21.05	−15.56	−15.05
Power law exponent for dislocation creep, n	4.0	4.2	3.5	3.5
Activation energy for dislocation creep, E_{Disloc} (kJ/mol)	223	445	530	480
Activation volume for dislocation creep, V_{Disloc} (cm^{-3})	0	0	13	10
Pre-exponential constant for Peierls creep, $\log(B_{Peierls})$ (Pa^{-n} s^{-1})	–	–	11.76	–
Activation energy for Peierls creep, $E_{Peierls}$ (kJ/mol)	–	–	540	–
Peierls stress, $\tau_{Peierls}$ (GPa)	–	–	8.5	–

is applied in order to track motion of the free surface and to prevent large grid distortion.

SLIM3D solves the conservation equations with simultaneous consideration of the constitutive laws using an implementation of elasto-visco-plastic rheology that decomposes the deviatoric strain rate into elastic, viscous, and plastic components (Simo and Hughes, 2000)

$$\dot{\varepsilon}_{ij} = \dot{\varepsilon}^{el}_{ij} + \dot{\varepsilon}^{vs}_{ij} + \dot{\varepsilon}^{pl}_{ij} = \frac{1}{2G}\tau^{*}_{ij} + \frac{1}{2\eta_{eff}}\tau_{ij} + \dot{\gamma}\frac{\partial Q}{\partial \tau_{ij}} \quad (4)$$

Where G is the elastic shear modulus, τ^*ij the objective stress rate, η_{eff} the effective creep viscosity, $\dot{\gamma}$ the plastic multiplier, and Q is the plastic potential function.

Following the approach of Kameyama et al. (1999), we use three types of solid state flow (diffusion, dislocation, and Peierls creep) to compute the effective viscosity

$$\eta_{eff} = \frac{1}{2}\tau_{II}\left(\dot{\varepsilon}_{Diff} + \dot{\varepsilon}_{Disloc} + \dot{\varepsilon}_{Peierls}\right)^{-1} \quad (5)$$

with τ_{II} being the second invariant of deviatoric stress. The individual strain rates are computed as follows:

Diffusion creep

$$\dot{\varepsilon}_{Diff} = B_{Diff}\tau_{II} \quad \exp\left(\frac{-E_{Diff}}{RT}\right) \quad (6)$$

Dislocation creep

$$\dot{\varepsilon}_{Disloc} = B_{Disloc}(\tau_{II})^{n} \quad \exp\left(\frac{-E_{Disloc}}{RT}\right) \quad (7)$$

Peierls creep

$$\dot{\varepsilon}_{Peierls} = B_{Peierls} \quad \exp\left[\frac{-E_{Peierls}}{RT}(1-\beta)^2\right]\left[\frac{\tau_{II}}{\beta\tau_{Peierls}}\right]^{\left(2\beta(1-\beta)\frac{E_{Peierls}}{RT}\right)} \quad (8)$$

Brittle deformation is implemented by means of the standard Mohr–Coulomb plasticity model:

$$A = \frac{1}{2}(\sigma_{max} - \sigma_{min}) + \frac{1}{2}(\sigma_{max} + \sigma_{min})\sin\varphi - c\cos\varphi \le 0 \quad (9)$$

where A defines the yield surface, σ_{max} and σ_{min} are maximum and minimum principal stresses, φ is the friction angle, and c cohesion.

The tectonic force F at the lateral boundaries is the key variable for the evaluation of the integrated lithospheric strength. It is computed by integrating the individual stresses of each boundary element (Brune et al., 2012 and references therein):

$$F = \sqrt{(S_{xx} - S_{zz})^2 + S^2_{xy} + S^2_{xz}} \quad \cdot \quad L_z \quad (10)$$

with

$$S_{ij} = \frac{1}{L_y L_z}\iint \sigma_{ij}\,dy\,dz \quad (11)$$

where the length of the model domain in y and z direction are denoted L_y and L_z, respectively.

Three major weakening mechanisms are included in the model which lead to localization within the lithosphere: (1) We use a strain-dependent friction coefficient which mimics the reduction of crustal fault strength (Popov et al., 2012; Provost and Houston, 2003; Zoback et al., 1987). The friction coefficient decreases linearly from 0.6 to 0.06 between 0 and 1 strain. (2) The shear heating term $\tau_{II}\dot{\varepsilon}_{II}$ in the energy conservation equation induces a positive feed-back loop: Large strain rates lead to increased temperature which lowers the effective viscosity. A smaller viscosity attracts deformation and thus increases the strain rate. (3) For a constant strain rate, the power law dependency of the dislocation creep leads to decreasing viscosity if stresses increase (i.e. stress softening). For constant stress on the other hand, the power law dependency results in lower viscosity for an increase in strain rate (i.e. strain rate softening).

3. Model setup

In this study we consider a rectangular segment of 1000 km length, 700 km width and 200 km depth (Fig. 2a). We assume a layered structure of the Earth (Fig. 2b) with a 20 km thick upper crust with wet quartzite rheology (Gleason and Tullis, 1995) and a lower crustal layer of 20 km thickness of granulite properties (Wilks and Carter, 1990). The mantle is incorporated as a (i) 60 km thick layer of strong mantle material and dry olivine rheology (Hirth and Kohlstedt, 2003) and (ii) asthenospheric mantle below 100 km depth where we apply rheological parameters of wet (i.e. 500 ppm H/Si) olivine that take into account the higher water content of the asthenosphere (Hirth and Kohlstedt, 2003). All rheological parameters are listed in Table 1.

Our numerical experiments incorporate both a rift zone and an erosional domain (Fig. 2c). Simulations are started with an equilibrium temperature distribution such that the 1350 °C isotherm outside the prospective rift zone is situated at 120 km depth, which accounts for thermal lithospheric thickness in non-cratonic continental environments (Artemieva., 2006). Moreover, a setting where the thermal lithosphere–asthenosphere boundary is located 20–30 km below the chemical lithosphere–asthenosphere boundary remains stable for several 100 Ma if small-scale convection is taken into account (Sobolev et al., 2009). Rifts often reactivate post-orogenic suture zones that bear a

Please cite this article as: Brune, S., et al., Quantifying the thermo-mechanical impact of plume arrival on continental break-up, Tectonophysics (2013), http://dx.doi.org/10.1016/j.tecto.2013.02.009

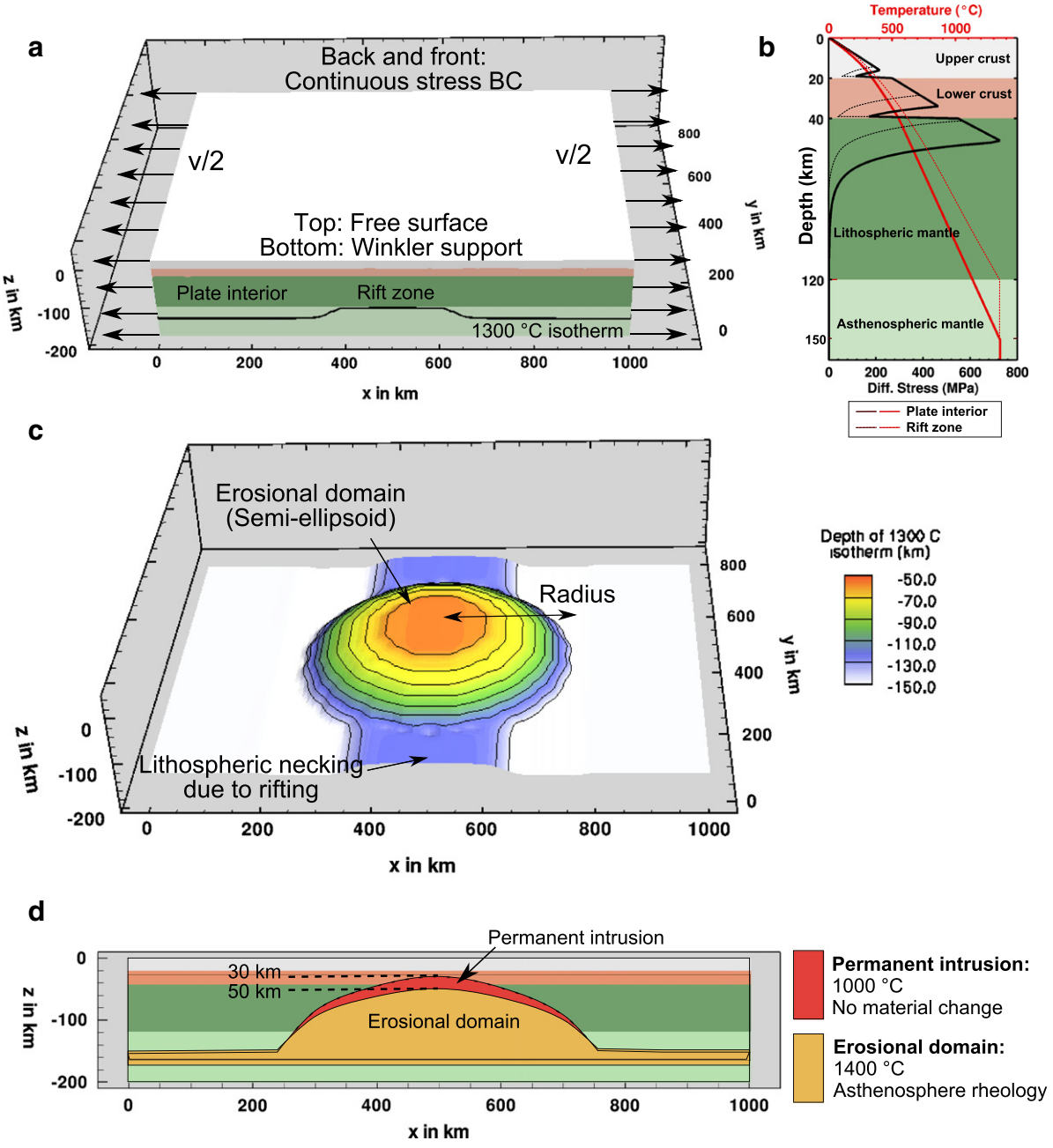

Fig. 2. (a) Initial and boundary conditions. Kinematic boundary conditions are applied at the faces in x-direction. (b) Initial yield stress envelopes. Rheological parameters are given in Table 1, details in text. (c) The shape of the area that was eroded by the plume head is approximated as semi-ellipsoid of specific radius and peak erosion depth. Spreading of the plume head below the lithosphere is approximated by a 20 km thick layer with the same parameters like the semi-ellipsoid. The initial lithospheric necking is used to focus extension in the rift center. (d) Cross section along x-direction showing the erosional domain and region of permanent intrusion.

characteristic weakness relative to undeformed neighboring lithosphere. Whether the reduced strength is caused by inherited crustal faults, higher density of radiogenic materials or mechanical anisotropy of the mantle lithosphere (Tommasi and Vauchez, 2001) is presently unclear. If the suture zone is thrown into extension, however, all of these processes lead to lithospheric necking and hot upwelling in the center of the rift. We mimic this process by initiating the rift via a small temperature deviation along strike: the 1350 °C isotherm is elevated from 120 km to 100 km in a region of 200 km width. The temperature below this surface is initially set to 1350 °C. The initial temperature distribution that is in equilibrium with respect to that isotherm relaxes self-consistently during further model evolution, where a constant temperature is applied at the top and bottom surfaces of the model (0 °C and 1350 °C, respectively). Zero heat flow conditions are imposed for lateral boundaries at all times.

Lithospheric erosion by a plume head is a complex dynamic process (Sobolev et al., 2011) that may generate multiple domains where the lithosphere is eroded due to repeated eclogitisation of mafic intrusions and subsequent delamination. In this study, we do not explicitely model erosion of the lithosphere by a plume that is assumed to be much faster than the rifting process (Sobolev et al., 2011). Instead, we approximate one of the eroded regions by a simple, semi-ellipsoid of distinct radius and a certain peak erosion depth (Fig. 2c). By varying these two parameters, we are able to evaluate the influence of the erosional domain geometry on the lithospheric strength while complex spatio-temporal variations are neglected. We further assume an asthenospheric rheology and a

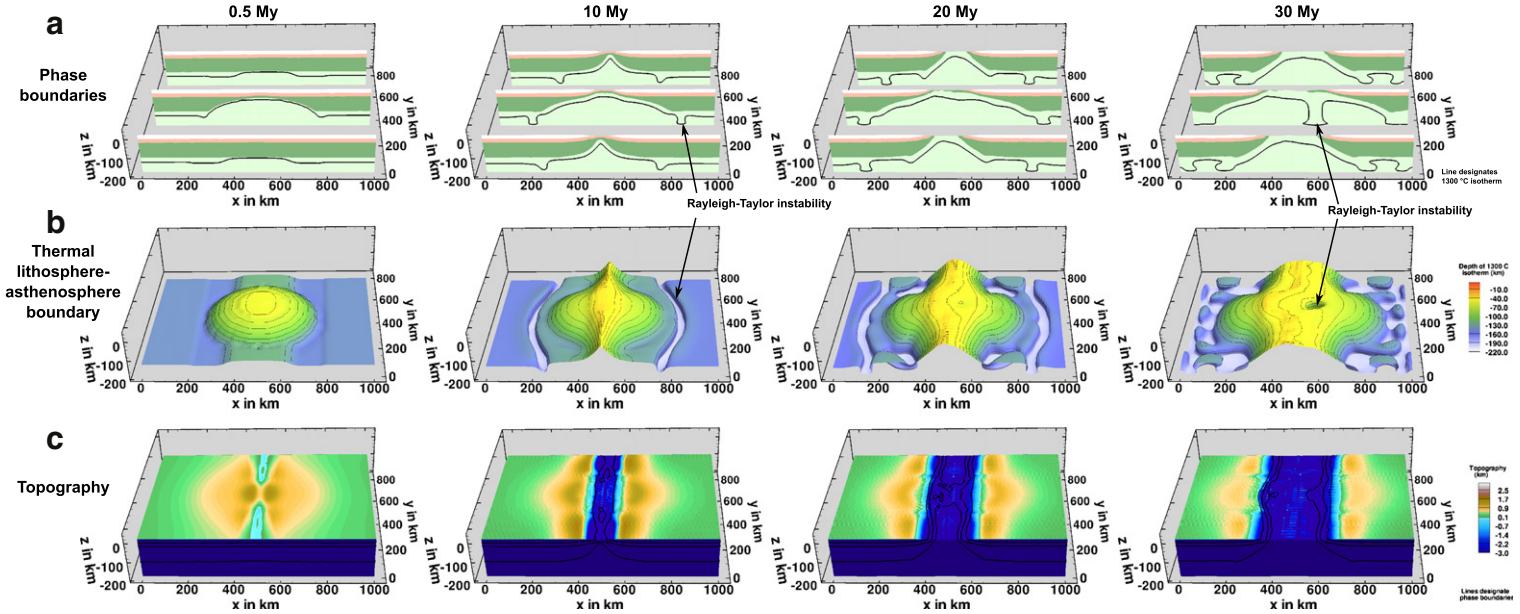

Fig. 3. Temporal evolution of a rift with an eroded area of 250 km radius, 50 km peak erosion depth, and 30 km permanent intrusion depth. (a) Vertical slices depict layering (for color scheme compare to Fig. 2) and 1300 °C isotherm as a black line. (b) Thermal lithosphere–asthenosphere boundary defined as 1300 °C isosurface. (c) Topography evolution. Black lines indicate phase boundaries. (For interpretation of the references to color in this figure legend, the reader is referred to the web version of this article.)

Please cite this article as: Brune, S., et al., Quantifying the thermo-mechanical impact of plume arrival on continental break-up. Tectonophysics (2013), http://dx.doi.org/10.1016/j.tecto.2013.02.009

temperature of 1400 °C inside the semi-ellipsoid, corresponding to 50 °C excess temperature with respect to the asthenosphere. Spreading of plume material below the lithosphere is implemented via a 20 km thick layer below the lithosphere with the same parameters like the semi-ellipsoid. Additional to the eroded domain, we take into account the presence of permanent (not delaminating) intrusions that are approximated by a second semi-ellipsoidal shape that is concentric to the first but reaches a depth of 30 km (Fig. 2d). Permanent intrusions strongly heat their surrounding which is incorporated in our model by elevating the temperature between both semi-ellipsoids to 1000 °C. The dimensions of the eroded domain and the temperature of the erosional and intrusional domain are based on Sobolev et al. (2011).

Mechanical boundary conditions for upper and lower faces are free surface at the top and Winkler support at the bottom. During each remeshing, the lower boundary is reset to 200 km, whereby markers (Lagrangian particles used to represent material advection) are either deleted or introduced. Extension is represented either by prescribing velocities at the boundaries perpendicular to the x-axis or by keeping the boundary force constant which allows for self-consistent evolution of extensional velocities. Throughout this publication, extension velocities refer to full spreading rates, so that extension of 10 mm/yr is realized by boundary velocities of 5 mm/yr at each side. Across the boundaries in y-direction we apply a continuous stress formulation, i.e. the face-parallel components of the stress tensor inside and outside the model domain are forced to be identical while non-zero face-perpendicular velocities are not allowed. This formulation is an extension of the free-slip boundary condition as the latter has the disadvantage that model boundaries are not able to sustain shear stresses and therefore represent enormous vertical faults cutting through the whole lithosphere.

We use cubic elements of 10 km edge length resulting in 140,000 elements within the computational domain. Due to the implicit time-stepping of SLIM3D, time steps of 20 ky can be used so that 1500 steps suffice to compute 30 My model time. The present version of SLIM3D solves the discretized conservation equations using the direct parallel shared memory solver PARDISO (Schenk and Gärtner, 2004).

4. Results

4.1. Rift evolution

The evolution of a rift system that is affected by lithospheric erosion is shown in Fig. 3. Extension is focused in the weakest part of the domain, i.e. the rift center, where hot asthenospheric upwelling occurs. The sides of the upwelling impose large gradients on the lithosphere–asthenosphere boundary (Fig. 3a) that facilitate foundering of the unstable lower lithosphere and the formation of small-scale convection cells. These areas where the upper, colder and hence denser lithospheric material drops in favor of hotter material below are visible in the 1300 °C isotherms of Fig. 3b. The evolution of surface topography is controlled both by plume and rift: As the plume-eroded lithosphere is replaced with hot asthenosphere, the surface is elevated isostatically up to 1.5 km, which is in good agreement to theoretical values of plume-related topography (Farnetani and Richards, 1994) and to previous 2D modeling results (Burov et al., 2007). Simultaneously, extensional crustal thinning leads to the formation of a rift valley. Both processes apply to different lateral scales which result in the superposition visible in Fig. 3c.

4.2. Geometry of erosional domain

Presently, there are no examples on Earth where a plume head is being impinged on the lithosphere and hence the size of the area where continental lithosphere is eroded is not accessible in situ. Passive continental margins whose break-up was influenced by plume activity deformed significantly during the ensuing rift process which makes it very difficult to assess width and height of the zone of interaction. Here, we vary the size of the plume–lithosphere interaction zone, represented by the semi-ellipsoid, and quantify the resultant effect on rift strength. To that aim, we evaluate the force that is required to maintain the prescribed rift velocity (Eq. (10)) and its evolution through time (Fig. 4). We compare two settings where permanent intrusions reach depths of 30 km or no permanent intrusion takes place. For each case, the radius is chosen to be both 100 km, and 250 km. During these calculations, the region inside the semi-ellipsoid is characterized by high temperature (1400 °C) and asthenospheric rheology (Table 1), while the permanently intruded area has a temperature of 1000 °C. Furthermore, we consider a simulation of pure rifting without any plume–lithosphere interaction as reference.

The maximum required force amounts to 28 TN/m for the case of unperturbed rifting (Fig. 4). If the erosion radius is 100 km, maximum forces are 27 TN/m without permanent intrusions, and 25.5 TN/m with intrusions. In the case of 250 km radius, the force amounts to 25 TN/m, and 22 TN/m, respectively. The force is obviously dependent on the length of the computational domain in y-direction. Rift domains outside the eroded region add significant strength to the overall force balance which also explains why the erosion-related force reduction amounts to only a few TN/m. Note however, that a single plume head may induce multiple erosional domains that would align along the rift (Sobolev et al., 2011). The required forces are large if compared to available tectonic forces (Buck, 2007). Thus, break-up will be possible only under occurrence of additional strength-reducing mechanism like rift obliquity (Brune et al., 2012; Heine and Brune, submitted for publication), significant input of melts via diking (Buck, 2004) or due to stress concentration.

Forces are lowered during the rift process as hot asthenospheric upwelling and crustal faulting reduce lithospheric strength in the center of the rift. Lithospheric necking is the main weakening mechanism whereas other strength-reducing processes like strain softening and shear heating contribute much less to force reduction (Brune et al., 2012). Interestingly, the necking width is independent of the erosional radius which explains why the influence of the erosional domain on the required force is restricted to the first 6 My (corresponding to 60 km extension). Thereafter, rift dynamics are controlled by lithospheric necking instead of plume-related erosion. For larger times and a mature rift system, all simulations exhibit forces below 7 TN/m that drop to very low values of 2–3 TN/m when crustal separation takes place and break-up is completed.

4.3. Force-limited environment

Relative plate velocities between two diverging continents result from a complex interplay of several factors like plate boundary forces, plate–mantle interaction, and lithospheric-scale weakening processes. If the modeled rift region is comparatively small with respect to the whole plate boundary it is appropriate to neglect its influence on the

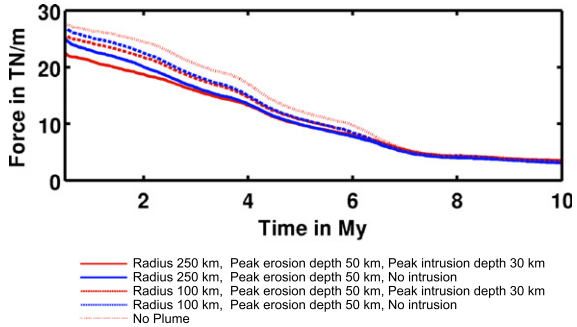

Fig. 4. Required force to maintain rift velocity over time. See Eq. (10) for definition of the force.

Please cite this article as: Brune, S., et al., Quantifying the thermo-mechanical impact of plume arrival on continental break-up, Tectonophysics (2013), http://dx.doi.org/10.1016/j.tecto.2013.02.009

plate-scale force balance so that the extensional velocity will be independent of the local lithospheric strength. However, if entire plate boundaries are modeled, or if the model region comprises an area that is crucial to the force balance (e.g. the last lithospheric connection between two continents), kinematics of the system will depend on the strength of the considered rift zone. In this case, force boundary conditions are feasible that allow to compute the time-dependent evolution of rift velocities.

In the previous section, we used velocities boundary conditions and computed the required force to maintain rifting. Now, assuming that plume arrival has a severe impact on the large-scale plate system (Fig. 1), we keep the boundary force constant and compute the model evolution for four different force values, namely 16 TN/m, 18 TN/m, 20 TN/m, and 22 TN/m (Fig. 5). In many cases, rift initiation predates plume arrival (Fig. 1) which is why we simulate plume impingement after a rift phase of 10 My. The radius of the eroded domain is 250 km and we consider a setup with lithosphere erosion and additional intrusions, a model with only lithosphere erosion, and a pure rift model that is not affected by a plume. Each model run evolves in three phases: (1) slow rifting with velocities below 10 mm/yr, (2) strong rift acceleration where velocities rise to 50 mm/yr within few million years, (3) a final rift and post break-up phase where the plate boundary strength is so low that relative plate velocities are no longer controlled by the local force-balance. In this final phase, where force boundary conditions are no longer physical, we limit the extensional velocity to typical sea-floor spreading rates of 50 mm/yr.

The key observable in this experiment is the timing of strong plate acceleration (Fig. 5). If forces are high, plate speed-up occurs earlier, while low boundary forces result in a very long low-velocity phase. The impact of plume-related lithosphere erosion on the rift dynamics becomes apparent if individual setups are compared for the same force: While for 22 TN/m (red lines), plume influence is negligible since the rift evolution is already very advanced at the moment of plume impingement, distinct differences are visible already for 20 TN/m (orange lines). Here, lithosphere erosion and intrusional heating result in about 7 My earlier break-up if compared to the setting without a plume. For 18 TN/m, the scenario without a plume does not lead to break-up within 30 My while the setups with lithosphere erosion accelerate at 14 My and 17 My. For 16 TN/m, plate motions accelerate after 23 My in the setup with both erosion and intrusion and after 28 My if only erosion is applied. This study shows that lithosphere erosion and intrusional heating may significantly accelerate the rift process. Under certain conditions where a pure rift without plume impingement would not be successful, they may even be a key factor in order to accomplish break-up. Within the force-limited setup, the observed delay between plume arrival and continental break-up (Fig. 1) can be explained by a comparatively low extensional force.

4.4. Relative influence of erosion, heating and topography on extensional force

A plume that erodes the lithosphere as modeled above, unites three different aspects that contribute to the local force balance: (1) It increases the temperature and thereby strongly reduces the temperature-dependent viscosity (Eqs. (5)–(8)). (2) It erodes strong lithospheric material which is replaced by weaker asthenosphere. (3) It generates topography that adds extensional stresses to the force balance. By varying our model with velocity boundary conditions, we can distinguish between the relative importance of these effects by respectively applying (or neglecting) (1) the semi-ellipsoidal domain of elevated temperature, (2) erosion inside the domain, and (3) a higher density within the erosional semi-ellipsoid that compensates for thermal expansion and hence does not elevate Earth's surface. We chose a density of 3325 kg/m^3 (instead of an asthenospheric density of 3300 kg/m^3) which allows to suppress plume-related topography. We stress that the high density is not the actual plume density itself, but constitutes an integrated value relating to a number of processes inside the eroded domain: eclogite formation and subsequent Rayleigh–Taylor instability, replacement by plume and asthenospheric material and crystallization to light garnet-free rocks. Assuming a higher density is useful in order to assess the influence of topography but also represents an important aspect of plumes that have a thermo-chemical nature.

We use all combinations of respectively switching temperature, erosion, and high density on and off, which, since it is not possible to use high density if no erosion occurs, results in six model setups (M1 to M6) that are illustrated in Fig. 6a. Note that temperature is represented by color, while boundaries between different material phases (upper and lower crust, lithospheric and asthenospheric mantle, plume-derived material of higher density) are depicted by solid black lines. We apply these six combinations to a setup with 250 km radius, peak erosion depth of 50 km and peak intrusion depth of 30 km (see solid red line in Fig. 4).

Our results show that temperature is the key factor in controlling lithospheric strength: The force curves (Fig. 6b) for all three scenarios with elevated temperature (solid lines) lie very close, M2 and M3 are even identical. The influence of topography can be deduced from comparing scenarios with and without high density, i.e. red lines

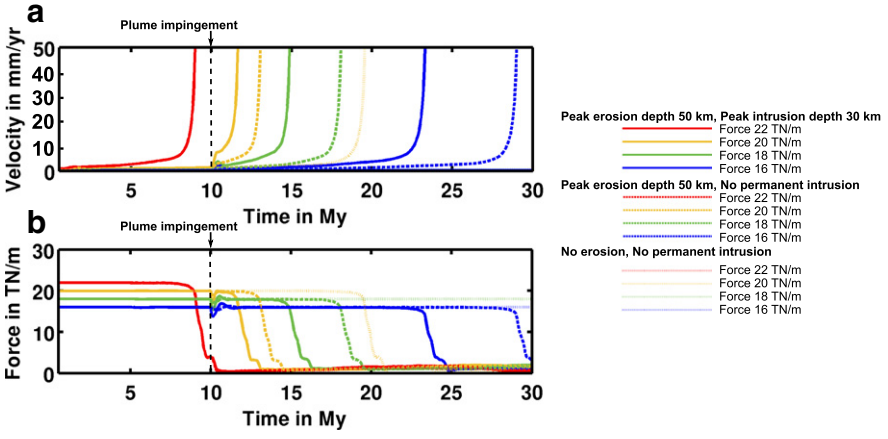

Fig. 5. Force boundary conditions. Velocities of each scenario evolve at constant force according to the strength of the system. Plume impingement takes place after an initial rift phase of 10 My. Line colors stand for different forces, while line style refers to different setups. Note that the scenarios with 22 TN/m (red line) evolve nearly identical since they reach the maximum velocity before plume impingement takes place. Scenarios with lower force evolve differently and this difference becomes larger the lower is the force. (For interpretation of the references to color in this figure legend, the reader is referred to the web version of this article.)

Please cite this article as: Brune, S., et al., Quantifying the thermo-mechanical impact of plume arrival on continental break-up, Tectonophysics (2013), http://dx.doi.org/10.1016/j.tecto.2013.02.009

and green lines. The difference between these curves does not exceed 2 TN/m. We conclude that although the generated topography reaches 1.5 km, it has only minor influence on the force balance. We consider the effect of lithosphere erosion and replacement by asthenosphere, by comparing green and blue lines. While there is a significant difference between M5 and M6 that both do not take the temperature effect into account, scenarios M2 and M3 are indistinguishable. Hence, the rheological effect of material exchange dominates only when the temperature effect is neglected. Summarizing these results, a hierarchy of controlling factors can be established: the temperature in the eroded region has first-order impact, the rheological difference is second order, and topographic effects have least influence on the force balance.

5. Discussion and conclusions

We have explored the three-dimensional thermo-mechanical effects of plume-related lithosphere erosion on rift strength and dynamics using a geodynamic elasto-visco-plastic model. Our model captures many effects of plume impingement on continental break-up: lithosphere erosion, asthenosphere heating, and intrusional lithospheric heating. Nevertheless, the important effect of diking (Buck, 2007) cannot yet be taken into account. Moreover, due to computational restrictions, our 3D model is limited to a single region of lithosphere erosion, while a plume head may generate multiple erosional domains (Sobolev et al., 2011). The spacing of these domains will have severe control on the strength evolution of the extensional system.

Keeping these model limitations in mind, we showed that lithosphere erosion may account for a force reduction of several TN/m. If translated to a force-limited setting this difference in strength may have significant impact on the timing of continental break-up, it may even control whether break-up takes place or not. Moreover, our experiments demonstrate that the interaction between lithosphere erosion and rifting generates complex topographic patterns resulting from superposition of rift and erosional effects. In terms of integrated rift strength, the temperature increase within the eroded domain has first

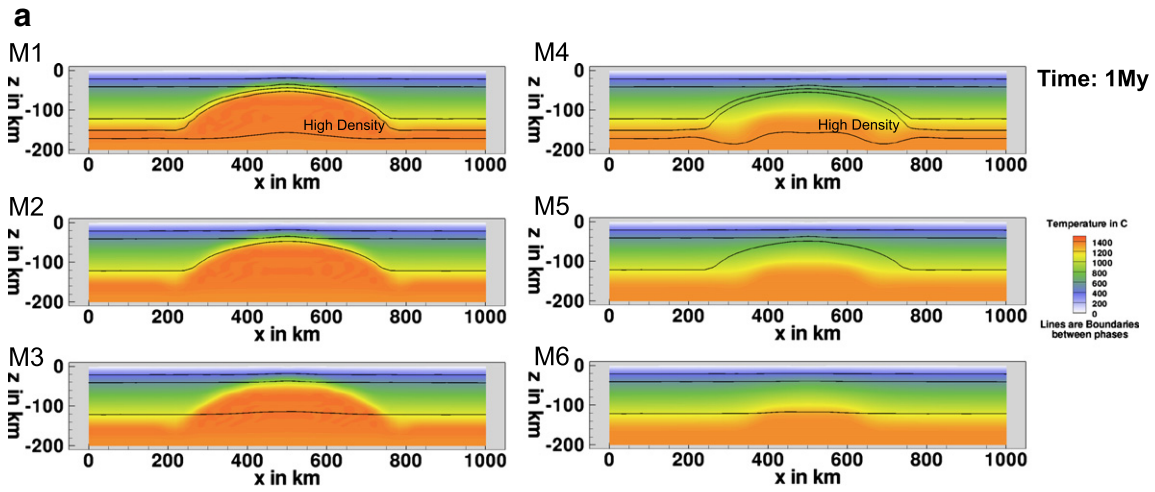

Fig. 6. Quantifying the effects of temperature elevation, lithosphere erosion and denser material within the eroded volume on the tectonic force.

Please cite this article as: Brune, S., et al., Quantifying the thermo-mechanical impact of plume arrival on continental break-up, Tectonophysics (2013), http://dx.doi.org/10.1016/j.tecto.2013.02.009

order impact, while material exchange is less important. We find that erosion-related isostatic topography plays only a minor role for the overall force balance.

Acknowledgments

This research is a product of SAMPLE (South Atlantic Margin Processes and Links with onshore Evolution), Priority Program 1375, funded by the German Research Foundation (DFG). We would like to thank the reviewer Taras Gerya for his suggestions that lead to significant improvements of the manuscript.

References

Allken, V., Huismans, R.S., Thieulot, C., 2011. Three-dimensional numerical modeling of upper crustal extensional systems. Journal of Geophysical Research 116, B10409.
Allken, V., Huismans, R.S., Thieulot, C., 2012. Factors controlling the mode of rift interaction in brittle–ductile coupled systems: a 3D numerical study. Geochemistry, Geophysics, Geosystems 13 (5), Q05010. http://dx.doi.org/10.1029/2012GC004077.
Artemieva, I.M., 2006. Global 1°×1° thermal model TC1 for the continental lithosphere: implications for lithosphere secular evolution. Tectonophysics 416 (1–4), 245–277.
Bassi, G., 1991. Factors controlling the style of continental rifting: insights from numerical modelling. Earth and Planetary Science Letters 105, 430–452.
Behn, M.D., Lin, J., Zuber, M.T., 2002. A continuum mechanics model for normal faulting using a strain-rate softening rheology: implications for thermal and rheological controls on continental and oceanic rifting. Earth and Planetary Science Letters 202, 725–740.
Bell, K., Castorina, F., Lavecchia, G., Rosatelli, G., Stoppa, F., 2004. Is there a mantle plume below Italy? Eos 85 (50), 541.
Braun, J., Beaumont, C., 1989. A physical explanation of the relation between flank uplifts and the breakup unconformity at rifted continental margins. Geology 17 (8), 760–764.
Brune, S., Autin, J., submitted for publication. The rift to break-up evolution of the Gulf of Aden: Insights from 3D numerical lithospheric-scale modelling. Currently in review at Tectonophysics
Brune, S., Popov, A.A., Sobolev, S.V., 2012. Modeling suggests that oblique extension facilitates rifting and continental break-up. Journal of Geophysical Research 117, B08402.
Buck, W.R., 1991. Modes of continental lithospheric extension. Journal of Geophysical Research 96, 20161–20178.
Buck, W.R., 2004. Consequences of asthenospheric variability on continental rifting. In: Karner, G.D., et al. (Ed.), Rheology and Deformation of the Lithosphere at Continental Margins. Columbia Univ. Press, New York, pp. 1–30.
Buck, W.R., 2007. Dynamic processes in extensional and compressional settings — The dynamics of continental breakup and extension. Treatise on Geophysics: Crust and Lithosphere Dynamics, vol. 6.
Buiter, S.J.H., Huismans, R.S., Beaumont, C., 2008. Dissipation analysis as a guide to mode selection during crustal extension and implications for the styles of sedimentary basins. Journal of Geophysical Research 113, B06406. http://dx.doi.org/10.1029/2007JB005272.
Burov, E., Cloetingh, S., 1997. Erosion and rift dynamics: new thermomechanical aspects of post-rift evolution of extensional basins. Earth and Planetary Science Letters 150, 7–26.
Burov, E., Guillou-Frottier, L., 2005. The plume head-continental lithosphere interaction using a tectonically realistic formulation for the lithosphere. Geophysical Journal International 161, 469–490.
Burov, E., Guillou-Frottier, L., d'Acremont, E., Le Pourhiet, L., Cloetingh, S., 2007. Plume head–lithosphere interactions near intra-continental plate boundaries. Tectonophysics 434, 15–38.
Chalmers, J.A., Larsen, L.M., Pedersen, A.K., 1995. Widespread Palaeocene volcanism around the northern North Atlantic and Labrador Sea: evidence for a large, hot, early plume head. Journal of the Geological Society 152, 965–969.
Choi, E., Lavier, L.L., Gurnis, M., 2008. Thermomechanics of mid-ocean ridge segmentation. Physics of the Earth and Planetary Interiors 171, 374–386.
Courtillot, V.E., Renne, P.R., 2003. On the ages of flood basalt events — Sur l'âge des trapps basaltiques. Comptes Rendus Geoscience 335, 113–140.
Courtillot, V., Jaupart, C., Manighetti, I., Tapponnier, P., Besse, J., 1999. On causal links between flood basalts and continental breakup. Earth and Planetary Science Letters 166, 177–195.
d'Acremont, E., Leroy, S., Burov, E.B., 2003. Numerical modelling of a mantle plume: the plume head–lithosphere interaction in the formation of an oceanic large igneous province. Earth and Planetary Science Letters 206, 379–396.
Dunbar, J.A., Sawyer, D.S., 1996. Three-dimensional dynamical model of continental rift propagation and margin plateau formation. Journal of Geophysical Research 101, 27845–27,863.
Elkins-Tanton, L.T., Hager, B.H., 2000. Melt intrusion as a trigger for lithospheric foundering and the eruption of the Siberian flood basalts. Geophysical Research Letters 27, 3937–3940.
Farnetani, C.G., Richards, M.A., 1994. Numerical investigations of the mantle plume initiation model for flood-basalt events. Journal of Geophysical Research, Solid Earth 99, 13813–13833.
Gac, S., Geoffroy, L., 2009. 3D Thermo-mechanical modelling of a stretched continental lithosphere containing localized low-viscosity anomalies (the soft-point theory of plate break-up). Tectonophysics 468 (1–4), 158–168.
Gerya, T., 2010. Dynamical instability produces transform faults at mid-ocean ridges. Science 329, 1047–1050.
Gerya, T., 2013. Three-dimensional thermomechanical modeling of oceanic spreading initiation and evolution. Physics of the Earth and Planetary Interiors 214, 35–42.
Gill, R.C.O., Holm, P.M., Nielsen, T.F.D., 1995. Was a short-lived Baffin Bay plume active prior to initiation of the present Icelandic plume? Clues from the high-Mg picrites of West Greenland. Lithos 34 (1–4), 27–39.
Gleason, G.C., Tullis, J., 1995. A flow law for dislocation creep of quartz aggregates determined with the molten-salt cell. Tectonophysics 247 (1–4), 1–23.
Golonka, J., Bocharova, N.Y., 2000. Hot spot activity and the break-up of Pangea. Palaeogeography, Palaeoclimatology, Palaeoecology 161, 49–69.
Heine, C., and Brune, S., submitted for publication. Oblique Rifting of the Equatorial Atlantic: why there is no Saharan Atlantic Ocean
Hirth, G., Kohlstedt, D.L., 2003. Rheology of the upper mantle and the mantle wedge: a view from the experimentalists. Geophysical Monograph 138.
Huismans, R.S., Beaumont, C., 2003. Symmetric and asymmetric lithospheric extension: relative effects of frictional-plastic and viscous strain softening. Journal of Geophysical Research 108 (B10), 2496. http://dx.doi.org/10.1029/2002JB002026.
Huismans, R.S., Beaumont, C., 2011. Depth-dependent extension, two-stage breakup and cratonic underplating at rifted margins. Nature 473 (7345), 74–78.
Kameyama, M., Yuen, D.A., Karato, S.I., 1999. Thermal–mechanical effects of low-temperature plasticity (the Peierls mechanism) on the deformation of a viscoelastic shear zone. Earth and Planetary Science Letters 168 (1–2), 159–172.
Katzman, R., ten Brink, U.S., Lin, J., 1995. Three-dimensional modeling of pull-apart basins: implications for the tectonics of the Dead Sea Basin. Journal of Geophysical Research 100, 6295–6312.
Lavier, L.L., Manatschal, G., 2006. A mechanism to thin the continental lithosphere at magma-poor margins. Nature 440, 324–328.
Lavier, L.L., Buck, W.R., Poliakov, A.N.B., 2000. Factors controlling normal fault offset in an ideal brittle layer. Journal of Geophysical Research 105, 23,431–23,442.
Le Pourhiet, L., Huet, B., May, D.A., Labrousse, L., Jolivet, L., 2012. Kinematic interpretation of the 3D shapes of metamorphic core complexes. Geochemistry, Geophysics, Geosystems 13, Q09002. http://dx.doi.org/10.1029/2012GC004271.
Moulin, M., Aslanian, D., Unternehr, P., 2010. A new starting point for the South and Equatorial Atlantic Ocean. Earth-Science Reviews 98 (1–2), 1–37.
Popov, A.A., Sobolev, S.V., 2008. SLIM3D: a tool for three-dimensional thermo mechanical modeling of lithospheric deformation with elasto-visco-plastic rheology. Physics of the Earth and Planetary Interiors 171 (1–4), 55–75.
Popov, A.A., Sobolev, S.V., Zoback, M.D., 2012. Modeling evolution of the San Andreas Fault system in northern and central California. Geochemistry, Geophysics, Geosystems 13 (8) doi:10.1029/2012GC004086.
Provost, A.-S., Houston, H., 2003. Stress orientations in northern and central California: evidence for the evolution of frictional strength along the San Andreas plate boundary system. Journal of Geophysical Research 108 (B3).
Regenauer-Lieb, K., Weinberg, R.F., Rosenbaum, G., 2006. The effect of energy feedbacks on continental strength. Nature 442, 67–70.
Rey, P.F., Teyssier, C., Kruckenberg, S.C., Whitney, D.L., 2011. Viscous collision in channel explains double domes in metamorphic core complexes. Geology 39, 387–390.
Schenk, O., Gärtner, K., 2004. Solving unsymmetric sparse systems of linear equations with PARDISO. Future Generation Computer Systems 20 (3), 475–487.
Schmeling, H., 2010. Dynamic models of continental rifting with melt generation. Tectonophysics 480 (1–4), 33–47.
Simo, J.C., Hughes, T.J.R., 2000. Computational Inelasticity, 2nd ed. Springer-Verlag, New York.
Sobolev, A.V., Sobolev, S.V., Kuzmin, D.V., Malitch, K.N., Petrunin, A.G., 2009. Siberian meimechites: origin and relation to flood basalts and kimberlites. Russian Gelogogy and Geophysics 50 (12), 999–1033.
Sobolev, S.V., Sobolev, A.V., Kuzmin, D.V., Krivolutskaya, N.A., Petrunin, A.G., Arndt, N.T., Radko, V.A., Vasiliev, Y.R., 2011. Linking mantle plumes, large igneous provinces and environmental catastrophes. Nature 477, 312–316.
Tommasi, A., Vauchez, A., 2001. Continental rifting parallel to ancient collisional belts: an effect of the mechanical anisotropy of the lithospheric mantle. Earth and Planetary Science Letters 185 (1–2), 199–210.
Ueda, K., Gerya, T., Sobolev, S.V., 2008. Subduction initiation by thermal–chemical plumes: numerical studies. Physics of the Earth and Planetary Interiors 171, 296–312.
Van Wijk, J.W., 2005. Role of weak zone orientation in continental lithosphere extension. Geophysical Research Letters 32 (2).
Van Wijk, J.W., Blackman, D.K., 2005. Dynamics of continental rift propagation: the end-member modes. Earth and Planetary Science Letters 229, 247–258.
Van Wijk, J.W., Cloetingh, S.A.P.L., 2002. Basin migration caused by slow lithospheric extension. Earth and Planetary Science Letters 198, 275–288.
Wilks, K.R., Carter, N.L., 1990. Rheology of some continental lower crustal rocks. Tectonophysics 182 (1–2), 57–77.
Ziegler, P.A., Cloetingh, S., 2004. Dynamic processes controlling evolution of rifted basins. Earth-Science Reviews 64, 1–50. http://dx.doi.org/10.1016/S0012-8252(03)00041-2.
Zoback, M.D., Zoback, M.L., Mount, V.S., Suppe, J., Eaton, J.P., Healy, J.H., Oppenheimer, D., Reasenberg, P., Jones, L., Raleigh, C.B., Wong, I.G., Scotti, O., Wentworth, C., 1987. New evidence on the state of stress of the San Andreas fault system. Science 238, 1105–1111.
Zuber, M.T., Parmentier, E.M., 1986. Lithospheric necking: a dynamic model for rift morphology. Earth and Planetary Science Letters 77, 373–383.

Please cite this article as: Brune, S., et al., Quantifying the thermo-mechanical impact of plume arrival on continental break-up, Tectonophysics (2013), http://dx.doi.org/10.1016/j.tecto.2013.02.009